Boundary modulation effects on MHD instabilities in Heliotrons

N.Nakajima 1), S.R.Hudson 2), C.C.Hegna 3), and Y.Nakamura 4)

1) National Institute for Fusion Science, Oroshi-cho 322-6, Toki 509-5292, Japan
2) Princeton Plasma Physics Laboratory, P.O.Box 451, Princeton NJ 08543, USA.
3) Department of Engineering Physics, University of Wisconsin-Madison, WI 53706, USA.
4) Graduate School of Energy Science, Kyoto University, Uji, Kyoto 611-0011, Japan

e-mail contact of main author : nakajima@nifs.ac.jp

Abstract In three-dimensional configurations, the confinement region is surrounded by the stochastic magnetic field lines related to magnetic islands or separatrix, leading to the fact that the plasma-vacuum boundary is not so definite compared with tokamaks that the various modulations of the plasma-vacuum boundary will be induced around the stochastic region by a large Shafranov shift of the whole plasma, in especially high-β operations. To examine such the modulation effects of the plasma boundary on MHD instabilities, high-β plasmas allowing a large Shafranov shift are considered in the inward-shifted LHD configurations with the vacuum magnetic axis R_{ax} of 3.6m, for which previous theoretical analyses indicate that pressure-driven modes are significantly more unstable compared with experimental observations. It is shown that the boundary modulation due to a free motion of the equilibrium plasma has not only significant stabilizing effects on ideal MHD instabilities, but also characteristics consistent to experimental observations.

1 Introduction

Recently, high-β plasmas with $\langle\beta\rangle \sim 3\%$ have been established in the inward-shifted configurations with the vacuum magnetic axis R_{ax} of 3.6m [1], for which previous theoretical ideal MHD stability analyses show that pressure-driven modes are significantly more unstable compared with experimental observations [2]. There may be two types of thought to remove this discrepancy between theoretical and experimental results. One is to show the nonlinear saturation level of the linear modes may be too low to influence on the confinement performance and/or to show some two-fluid or kinetic effects added to MHD model may have strong stabilizing effects. The other is to reconsider the MHD equilibria themselves used in the linear and nonlinear stability analyses. It should be noted that, in the previous theoretical considerations, the MHD equilibria are mainly calculated under a fixed boundary corresponding to a *clear* Last Close Flux Surface (LCFS) of the vacuum magnetic field [2,3], and that, in the free boundary equilibrium calculations, an artificial material limiter is introduced to fix the plasma boundary, where the plasma pressure vanishes, on the clear LCFS of the vacuum magnetic field in the outboard of the horizontally elongated poloidal cross section [4]. Those methods to determine the MHD equilibria are based on the conjecture that the plasma do not expand beyond the clear LCFS of the vacuum field so much. In these analyses, the resultant MHD equilibria are strongly unstable against the pressure-driven ideal MHD modes in the inward-shifted LHD configurations. However, such a clear LCFS of the vacuum magnetic field is surrounded by unclear flux surfaces or stochastic magnetic field lines with a quite long connection length and a definite rotational transform, namely *averaged flux surfaces* with a quite long connection length and a definite rotational transform could exist in such a stochastic region. Thus, it is natural to consider that a movement of the equilibrium plasma into such a region is allowable and that a boundary modulation induced by the plasma free motion will lead to a state with lower free energy compared to that under the fixed boundary. Indeed, experimentally, it is fairly standard observation that the stochastic magnetic region surrounding nested flux surfaces holds confinement properties or pressure gradient due to long connection lengths of the magnetic field lines related to some magnetic structures [5].

In this work, analyses on MHD equilibria and stability are performed in order to show the significant stabilizing effects of the boundary modulation due to a free motion of equilibrium plasma with increasing β on the linearized ideal MHD stability, which may lead to removal of discrepancy between experimental and the previous theoretical results. For the MHD equilibrium calculations, vmec code [6]is used, where only currentless equilibria are considered for simplicity. For linearized ideal MHD stability analyses, cas3d3 code [7], based on the variational or energy principle, is used for low-n compressible or incompressible perturbations (n is the toroidal mode number), under the constant mass density assumption.

2 Properties of the peripheral magnetic field

2.1 Vacuum magnetic field

The Poincare plots of the peripheral vacuum magnetic field in the horizontally elongated LHD poloidal cross section are shown in upper row of Fig. 1, for inward-shifted (left), standard (middle), and outward-shifted (right) configurations.

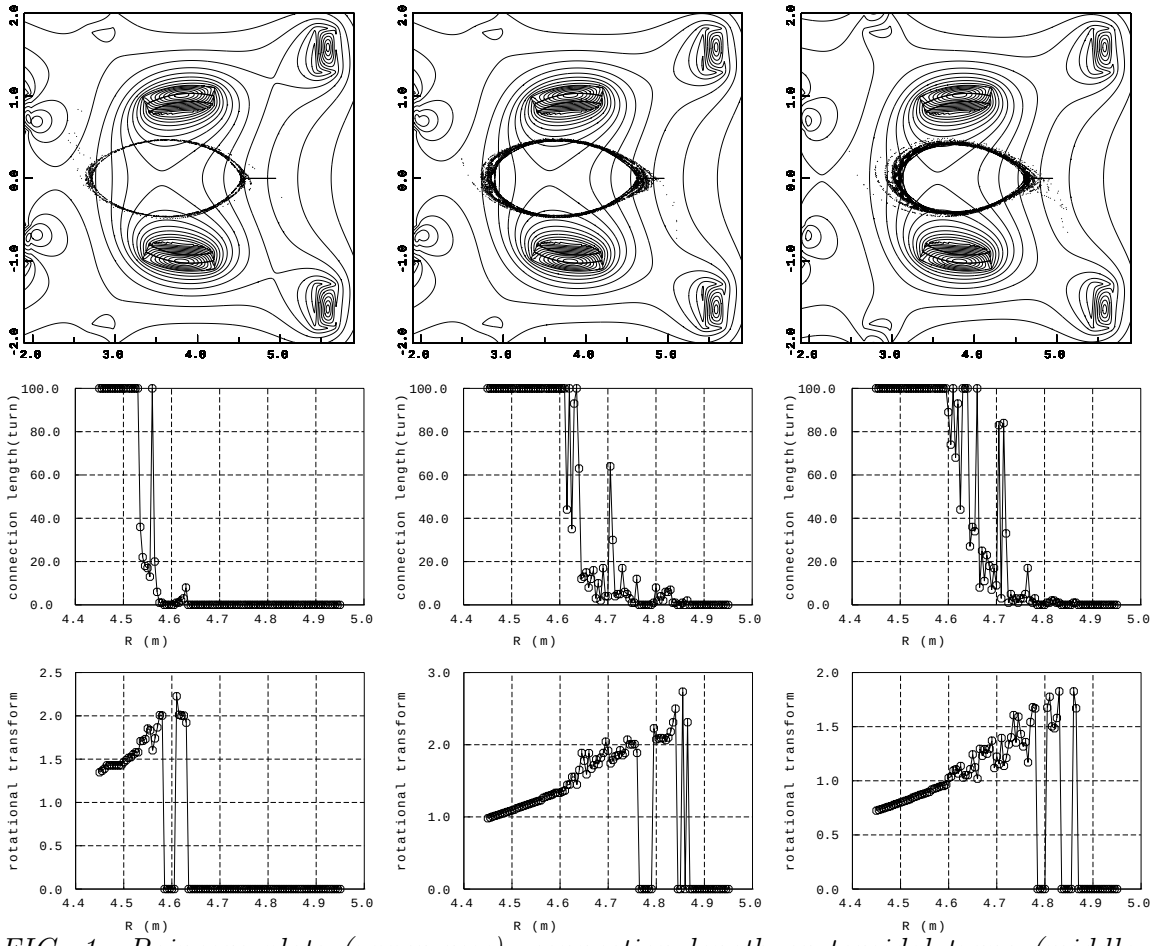

FIG. 1: Poincare plots (upper row), connection length or toroidal turns (middle row), and rotational transform ι (lower row). Three columns correspond to inward-shifted (left), standard (middle), and outward-shifted (right) configurations. In the Poincare plots, the contours of magnetic field strength and the shape of helical coils are also shown by thin and thick solid lines, respectively.

From these figures, it is understood that the width of the peripheral region with stochastic magnetic field lines changes thick to thin according to the vacuum magnetic axis shift from outboard to inboard. The inward-shifted configurations are characterized as the configurations

with most thin width of the peripheral stochastic region. The middle row of Fig. 1 indicates the corresponding connection length (toroidal turn) of the magnetic field lines started from the equatorial plane ($z = 0$) as a function of the major radius R. The corresponding rotational transform ι is denoted in the lower row of Fig. 1, where ι is set 0 when the connection length is shorter than one toroidal turn. From these two types of figures, it is understood that the region with a fairly long connection length (more than 100 toroidal turns ~ 2.2 km) is limited by magnetic islands with $\iota = 30/19 \sim 1.579$ (inward-shifted), $\iota = 20/15 \sim 1.333$, (standard) and $\iota = 10/10 = 1$ (outward-shifted). In the inward-shifted configurations, a clear LCFS might be chosen around $\iota = 1.48$ near the magnetic island with $\iota = 30/20$.

The region with a quite short connection length, for example, less than one toroidal turn, is considered to be direct loss region without plasma confinement. In contrast with it, the region with a long connection length and a definite rotational transform is considered to become a plasma confinement region with *averaged flux surfaces* depending on electron temperature and electron density there. Since the typical mean free path along a magnetic field line is around $10 \sim 20$ m, the stochastic region consisting of field lines with a connection length of several 10 turns might be considered to be a confinement region with anomalous diffusion properties. Letting the magnetic field in this region be $\vec{B} + \delta\vec{B}$ where $\vec{B}$ and $\delta\vec{B}$ are an averaged regular magnetic field and a fluctuating magnetic field, respectively, the electron thermal diffusion coefficient χ_e might be estimated as

$$\chi_e = \frac{4 v_{Te} \delta k_{||}}{\pi^{3/2} \overline{k}_r^2} \begin{cases} \mathcal{R}^2 & \text{for} \quad \mathcal{R} \le 1 \\ \mathcal{R} & \text{for} \quad \mathcal{R} \ge 1, \end{cases} \qquad \mathcal{R} \equiv \left[\frac{\pi}{8} \frac{L_{||} \overline{k}_r^2}{\delta k_{||}} \sum_m \left\langle \left(\frac{\delta B_{rmk_{||}}}{B} \right)^2 \right\rangle_{k_{||}} \right]^{1/2} \tag{1}$$

where $L_{||}$ and $\delta k_{||} \sim L_{||}^{-1}$ is the parallel correlation length and the width of the parallel wave numbers contributing to the diffusion, respectively, and $L_\perp$ and $\overline{k}_r \gtrsim L_\perp^{-1}$ are the perpendicular (radial) correlation length and the typical radial wave number, respectively. $\delta B_{rmk_{||}}$ means the Fourier component of a radial fluctuating magnetic field with the poloidal mode number m and the parallel wave number $k_{||}$, and v_{Te} is an electron thermal velocity. The formula given by Eq.(1) is derived from the Lagrange auto-correlation function by following the particle orbits without toroidal drift, where a renormalization effect is included and $\mathcal{R} \ll 1$ corresponds to the quasi-linear limit. When the magnitude of the fluctuating magnetic field $\delta\vec{B}$ is sufficiently small compared with the averaged regular field $\vec{B}$, the region with stochastic magnetic field lines might be treated as a confinement region with the electron thermal diffusion coefficient χ_e given by Eq.(1). Based on this fact, the plasma-vacuum boundary could be chosen from averaged flux surfaces with a long connection length and a definite rotational transform in the stochastic region, and also a free equilibrium plasma motion could be allowed in such a stochastic region through the change of the vacuum magnetic field by the plasma current.

2.2 Finite-β magnetic field

Properties of the peripheral magnetic field of finite-β MHD equilibria are investigated by using HINT2 code (a new version of the original HINT code [8]). In HINT2 code, as well as HINT code, a relaxation method is used in order to obtain the MHD equilibrium without the assumption of the nested flux surfaces. Although the boundary of the calculation box is assumed to be a perfect conductor, the obtained MHD equilibrium is essentially free boundary equilibrium because no fixed boundary condition is introduced between plasma region and the vacuum region. The relaxation method is an iterative method consisting of 1) parallel relaxation of the pressure along fixed magnetic field lines and 2) perpendicular relaxation of the magnetic field for a fixed pressure profile. The parallel relaxation introduces an effective perpendicular transport of the pressure with respect to an averaged magnetic field $\vec{B}$, when

the magnetic field is decomposed into an averaged regular part $\vec{B}$ and a fluctuating part $\delta\vec{B}$ (for clear nested flux surfaces, $\delta\vec{B} = 0$, so that there is no effective perpendicular transport). In such cases, the effective perpendicular transport coefficient $\chi_\perp$ is proportional to χ_e given by Eq.(1). Moreover, since the plasma pressure along the magnetic field lines with a short connection length is reset to 0, only the pressure along magnetic field lines with a long connection length is kept in the resultant MHD equilibrium.

Figure 2 shows the Poincare plots of the magnetic field lines of the finite-β plasma for $\langle\beta\rangle = 1.4\%$ (left column) and $\langle\beta\rangle = 3.7\%$ (right column) in the inward-shifted configuration. As β increases, the width of the peripheral magnetic islands becomes wide, and stochastic magnetic field is created near the plasma periphery through islands-overlapping. Such a stochastic region penetrates from the plasma peripheral region to core region, as β increases. The pressure gradient still exists in the stochastic region with a long connection length and a definite rotational transform, and so, as well as the vacuum magnetic field, such a stochastic region should be treated as the plasma region with averaged flux surfaces.

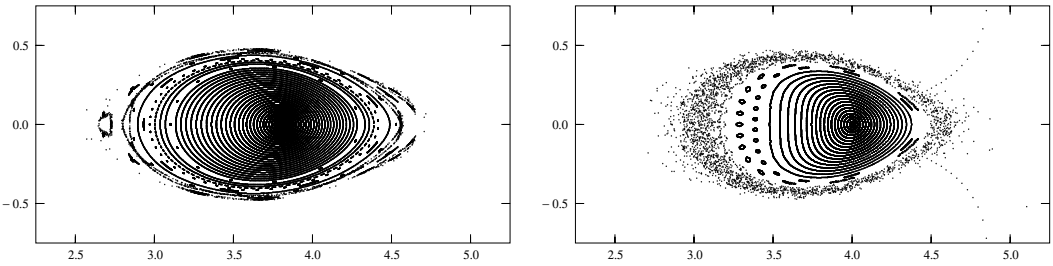

FIG. 2: Poincare plots of the magnetic field lines in the horizontally elongated LHD poloidal cross section for $\langle\beta\rangle = 1.4\%$ (left column) and $\langle\beta\rangle = 3.7\%$ (right column).

3 Properties of the ideal MHD stability

According to the consideration in the previous section, several MHD equilibria in the inward-shifted LHD configuration are chosen for linearized ideal MHD stability analyses. Essential point of the consideration is that the an averaged flux surface could be chosen as a plasma-vaccum boundary from the region with stochastic magnetic field lines, when the connection length is long and the rotational transform is definite. However, there is still ambiguity which surface should be chosen. Moreover, it is not so easy to distinguish stabilizing or destabilizing effects due to the change of the local pressure gradient on the mode rational surface from those due to the geometrical change induced by the plasma free boundary motion. Thus, two types of approaches are chosen to specify the MHD equilibrium. One is to simulate the effects of the free boundary motion by introducing small boundary modulation to the boundary determined from the vacuum magnetic field. In this cases, change of stabilizing or destabilizing effects due to the change of the local pressure gradient on the rational surfaces related to unstable modes is so weak that almost pure effects due to the boundary modulation on MHD stability might be observed. The other one is natural free boundary equilibrium calculations, where several averaged flux surfaces are chosen for comparison.

3.1 In MHD equilibria with modulated fixed boundary

In the inward-shifted LHD configurations, the vacuum flux surfaces are so compressed into the helical coils inner side of torus that the bumpy deformation of the plasma boundary, expressed by the Fourier components with $(m, n) = (0, \neq 0)$ (m and n are poloidal and toroidal mode numbers, respectively) is strongly enhanced. As β increases, the whole plasma moves from inner side of the torus to the outer side. Through this Shafranov shift, the enforced boundary shaping by external coils will be so reduced that the bumpy deformation of the plasma

boundary will diminish. In order to simulate the effects of the boundary modulation related to the bumpy components induced by the free boundary motion, four types of currentless MHD equilibria with different plasma boundary shapes, shown in Tab.1, are investigated under the fixed boundary condition for various β-values by using vmec code. The boundaries of Type S and L are determined from the vacuum nested flux surfaces without boundary modulations, where S and L indicate small and large plasma volume, respectively. The rotational transform at the plasma boundary is $\iota = 1.36$ for Type S and $\iota = 1.48$ for Type L, respectively. On the other hand, the boundaries of Type *S-mod* and *L-mod* are created from those of Type S and L by eliminating only the bumpy Fourier components from the plasma boundary spectrum. Broad pressure profiles, which is considered to be similar to experimentally obtained one, $P(s) = P_0(1-s)(1-s^9)$ is used, where is s is the normalized toroidal flux. The ideal MHD stability analyses for compressible perturbations are performed by using the cas3d3 code.

Type	S	L	*S-mod*	*L-mod*
boundary	vacuum	vacuum	modified S	modified L

TAB. 1 Boundary type of considered MHD equilibria

Figure 3 shows the contours of the flux surfaces and level surfaces of the vmec poloidal angles in the vertically elongated poloidal cross section of vacuum (left column) and finite-β with $\langle\beta\rangle = 3.0\%$ (right column) configurations with original L (upper row) and modulated *L-mod* (lower row) plasma boundary. It is understood from these figures that although the change of the plasma boundary shape by eliminating the bumpy components from the plasma boundary spectrum is quite small, considerable outward magnetic axis shift is induced.

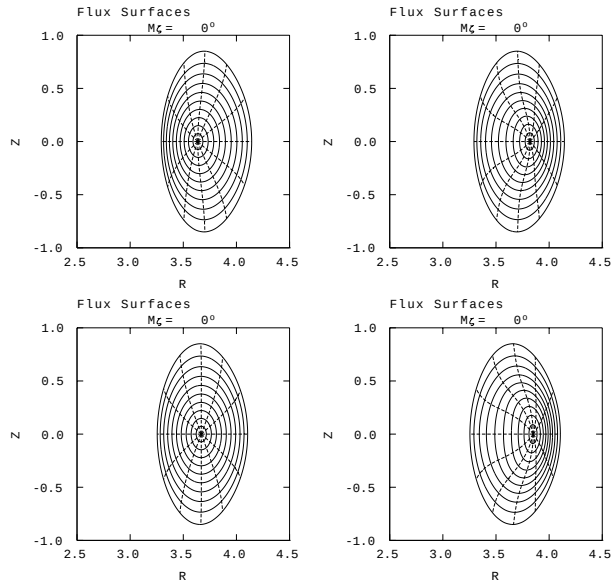

FIG. 3: Contours of the flux surfaces and level surfaces of the vmec poloidal angles in the vertically elongated poloidal cross section for vacuum (left column) and finite-β with $\langle\beta\rangle = 3.0\%$ (right column) configurations with original L (upper row) and modulated L-mod (lower row) plasma boundary.

This geometrical change of the flux surfaces leads to the significant change of the Mercier criterion as is shown in Fig. 4. Since the pressure gradient on each flux surface is fixed and ι does not change so much, the change of the Mercier criterion D_I is considered to mainly come from the geometrical effects induced by the boundary modulation.

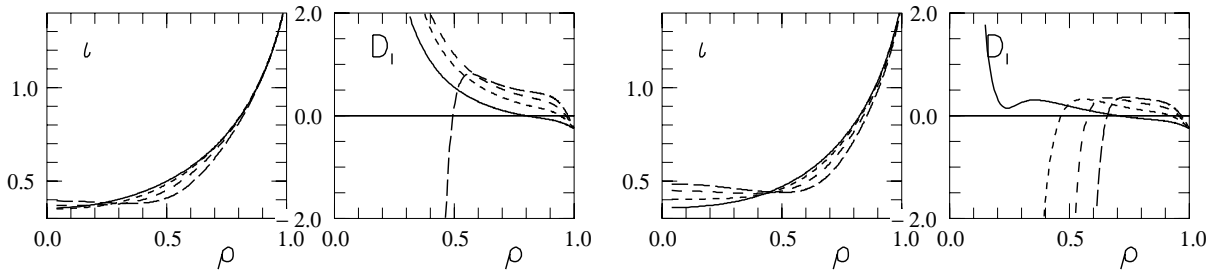

FIG. 4: Change of the rotational transform ι and the Mercier criterion D_I with respect to $\langle\beta\rangle$ for original L (left two columns) and modulated L-mod (right two columns) configurations, where $\rho = \sqrt{s}$. Solid lines correspond to the vacuum. Dashed lines correspond to $\langle\beta\rangle = 1\%$, $\langle\beta\rangle = 2\%$, and $\langle\beta\rangle = 3\%$ from short to long ones.

Figure 5 shows the growth rates normalized by the Alfvén transit time on the magnetic axis $\gamma\tau_{A0}$ vs the toroidal mode number n for equilibria with original vacuum boundary (Type S and L), where $\gamma\tau_{A0} = 0.1$ corresponds to around 40μsec for typical high-β LHD operation parameters. Every magnetic field line at a Mercier unstable rational surface has unfavorable magnetic curvature in average, and so the toroidal mode coupling of perturbations inherent to helical systems becomes so weak there [9,10]that the toroidal mode number n can be used as a good quantum number. As β increases, unstable modes change from localized interchange modes with only single dominant Fourier mode, to localized interchange modes consisting of multiple Fourier components, and finally to ballooning modes, except for considerably low-n modes, say, $(m, n) = (2, 1)$. As is understood from the comparison of stability analyses between fixed boundary (left column in Fig. 5) and free boundary (right column in Fig. 5), the perturbations become significantly more unstable and more global, when free radial motions of the perturbations are allowed on the plasma boundary, because such free motions lead to the excitation of the Fourier modes resonating near the plasma edge and the possibility that low-n global interchange modes under the fixed boundary condition with $\xi^s(a) = 0$ change into ballooning modes for $\xi^s(a) \neq 0$, where $\xi^s = \vec{\xi}\cdot\nabla s$ is the normal component of the displacement vector $\vec{\xi}$.

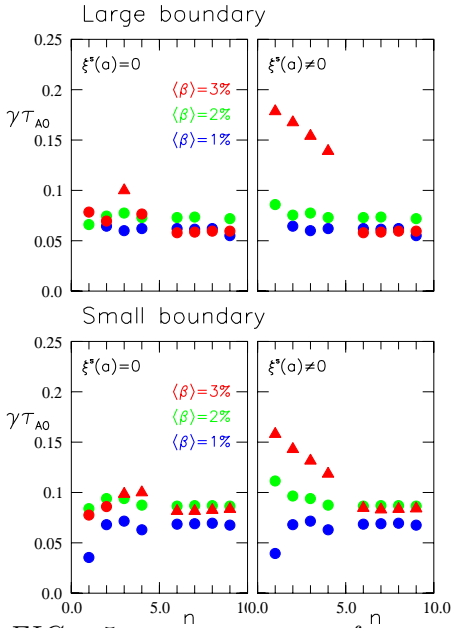

FIG. 5: $\gamma\tau_{A0}$ vs n for equilibria with original vacuum boundary (Type S (lower row) and Type L (upper row)). The left (right) column corresponds to fixed (free) boundary stability analyses. The circles (triangles) denote interchange (ballooning) modes.

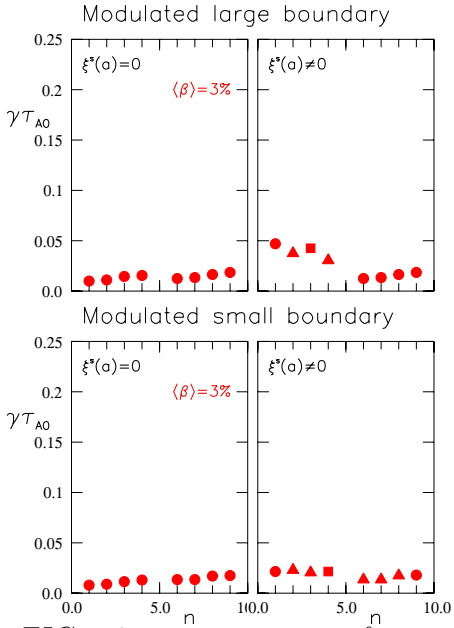

FIG. 6: $\gamma\tau_{A0}$ vs n for equilibria with modulated boundary (Type S-mod (lower row) and Type L-mod (upper row)) and $\langle\beta\rangle = 3\%$. The notations are same as Fig. 5, and additional rectangles indicate ballooning modes with external components.

Figure 6 shows $\gamma\tau_{A0}$ vs n for equilibria with modulated boundary Type *S-mod* or Type *L-mod*. Significant stabilizing effects by the boundary modulation simulating the free boundary motion of equilibrium plasma are quite clear. The stability properties between Type S and Type L boundary, and between Type *S-mod* and Type *L-mod* boundary do not change so much that it may be concluded that the size effects of the plasma boundary are weak. It should

be emphasized that a small change of the boundary shape leads to the significant improvement of the MHD stability through the geometrical change of the MHD equilibrium brought by the Shafranov shift.

One of characteristic points are that the experimentally observed modes with $(m, n) = (2, 3)$ [11], whose resonant surface may be considered to be outside of the plasma, are weakly excited like external modes as is shown in Fig. 7. Since the magnitude of vacuum magnetic perturbations is determined by the ξ^s on the plasma-vacuum surface, $(m, n) = (2, 3)$ mode is dominantly observed in these perturbations.

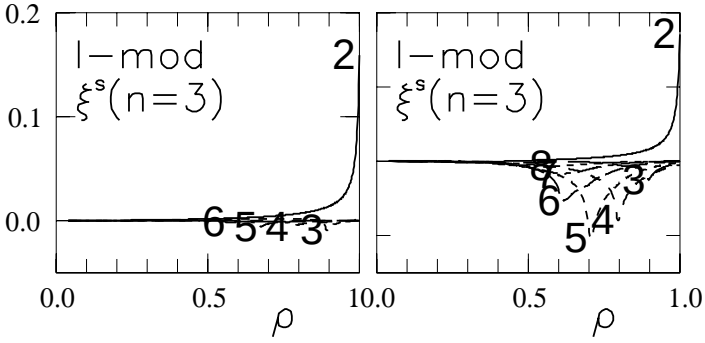

FIG. 7: Radial profiles of Fourier component of eigenfunctions with an external Fourier component: $(m, n) = (2, 3)$ for $\langle\beta\rangle = 2\%$ (left column) and $\langle\beta\rangle = 3\%$ (right column) equilibria with boundary Type L-mod. Attached numbers indicate the poloidal mode numbers m.

The other characteristic points is that the core region stays in the second stability region of the ballooning modes. This point will be intensively examined in near future.

3.2 In MHD equilibria with free boundary

Free boundary currentless equilibria in various β values are created by keeping the contained toroidal flux constant. Each contained toroidal flux corresponds to the vacuum rotational transform $\iota_v = 1.48$, $\iota_v = 1.58$, and $\iota_v = 1.72$. The surface corresponding to $\iota_v = 1.48$ is a clear nested flux surface, however, surfaces corresponding to $\iota_v = 1.58$, and $\iota_v = 1.72$ are averaged flux surfaces existing in the stochastic magnetic field region. Corresponding ι in finite-β equilibria with $\langle\beta\rangle = 3\%$ are $\iota = 1.49$, $\iota = 1.60$, and $\iota = 1.77$, respectively, where the same pressure profile as that in the previous cases is used. In order to distinguish effects of the equilibrium free motions on MHD stability from stability properties in the fixed boundary MHD equilibria, corresponding fixed plasma boundaries are created from the free boundary equilibrium with a quite low plasma pressure. Hereafter, only free boundary stability analyses are done for incompressible perturbations. Roughly speaking, the growth rate of the compressible perturbation is one-third of that of the incompressible perturbation. Figure 8 shows the comparison of stability analyses between fixed boundary MHD equilibria and free boundary MHD equilibria. As well as the MHD equilibria with boundary modulation, free boundary MHD equilibria are quite stable compared with the corresponding MHD equilibria with fixed boundary. By comparing Fig. 8 with the right column of Fig. 5 and Fig. 6, it is understood that significant stabilizing effects by a free motion of MHD equilibrium related to the Shafranov shift mainly correspond to the elimination of the bumpy components from the plasma boundary ($\gamma\tau_{A0}$ for compressible perturbations is around one-third of that for incompressible perturbations).

One of characteristics of the stability analyses for free boundary MHD equilibria is that interchange modes with an external Fourier component of $(m, n) = (1, 2)$ are excited, when a larger plasma boundary is chosen as shown in Fig. 9. These modes are recently observed in an inward-shifted configuration with a little bit different coil aspect ratio. In this perturbation given in Fig. 9, $(m, n) = (1, 2)$ mode may be dominantly observed experimentally.

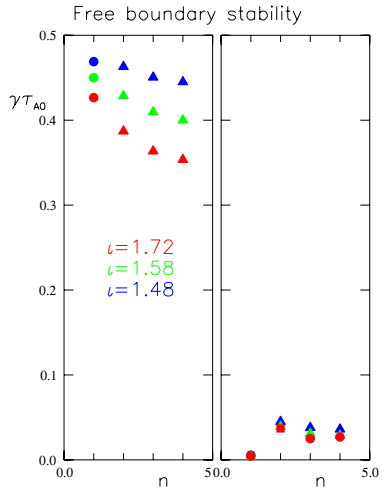

FIG. 8: $\gamma\tau_{A0}$ vs n for MHD equilibria ($\langle\beta\rangle$ = 3%) with fixed boundary (left column) and with free boundary (right column). Blue, green, and red colors correspond to the equilibrium with the rotational transform at the plasma boundary of ι_v = 1.48, ι_v = 1.58, and ι_v = 1.72 in the vacuum states. Circles (triangles) denote interchange (ballooning or ballooning-like) modes. The red square indicates the interchange modes with external Fourier component shown in Fig. 9.

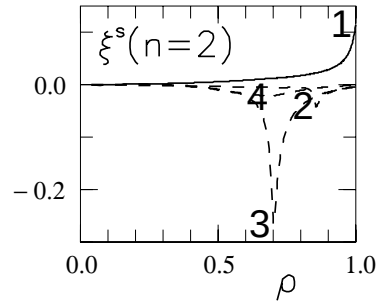

FIG. 9: Radial profiles of Fourier components of eigenfunctions with an external Fourier component: $(m, n) = (1, 2)$ for the free boundary MHD equilibrium with ι_v = 1.72 and $\langle\beta\rangle$ = 3%, which corresponds to the growth rate denoted by red square in Fig. 8. Attached numbers denote the poloidal mode numbers m.

4 Discussions

It has been shown that the boundary modulation by a free motion of MHD equilibrium related to Shafranov shift has significant stabilizing properties for ideal pressure-driven modes, where essential modulation is reduction of the bumpy components of the plasma boundary. These stabilizing effects do not depend on the choice of the averaged flux surfaces with a long connection length and a definite rotational transform from the vacuum magnetic field. Depending on the chosen boundary, however, various external modes, which have same Fourier spectrum as those experimentally observed, are excited. In experiments, both the plasma boundary and the pressure profile will change in β ramp-up phases, according to the heating and the density control. Adequate choice of the plasma boundary and pressure profile might lead to better coincidences between theory and experiment.

The author(N.N) greatly acknowledges Dr.K.Y.Watanabe for his quite fruitful discussions.

References

[1] MOTOJIMA, O., et al., Nucl. Fusion **43** (2003) 1674.
[2] NAKAJIMA, N., To appear in J.Plasma Fusion and Res. SER. **6** (2004).
[3] ICHIGUCHI, K., NAKAJIMA, N., et al., Nucl. Fusion **33** (1993) 481.
[4] ICHIGUCHI, K., NAKAJIMA, N., and GARDNER, H. J, Nucl. Fusion **36** (1996) 1157.
[5] MORISAKI, T., et al., J. Nucl. Materials **313-316** (2003) 548.
[6] HIRSHMAN, S. P., Phys. Fluids **26** (1983) 3553.
[7] NÜHRENBERG. C, Phys. Plasmas **6** (1999) 137.
[8] HARAFUJI, K, et al., J. Comput. Phys. **81** (1989) 169.
[9] NAKAJIMA, N, Phys. Plasmas **3** (1996) 4556.
[10] CHEN, J., NAKAJIMA, N, and OKAMOTO, M., Phys. Plasmas **6** (1999) 1562.
[11] SAKAKBARA, S., et al., Plasma Phys. Control. Fusion **44** (2002) A217.